

On the Paramount Role of Absorber Stoichiometry in (Ag,Cu)(In,Ga)Se₂ Wide-Gap Solar Cells


Jan Keller,* Lars Stolt, Kostiantyn V. Sopiha, Jes K. Larsen, Lars Riekehr, and Marika Edoff

This contribution evaluates the effect of absorber off-stoichiometry in wide-gap (Ag,Cu)(In,Ga)Se₂ (ACIGS) solar cells. It is found that ACIGS films show an increased tendency to form ordered vacancy compounds (OVCs) with increasing Ga and Ag contents. Very little tolerance to off-stoichiometry is detected for absorber compositions giving the desired properties of 1) an optimum bandgap (E_G) for a top cell in tandem devices ($E_G = 1.6\text{--}1.7\text{ eV}$) and at the same time 2) a favorable band alignment with a CdS buffer layer. Herein, massive formation of either In- or Ga-enriched OVC patches is found for group I-poor ACIGS. As a consequence, carrier transport and charge collection are significantly impeded in corresponding solar cells. The transport barrier appears to be increasing with storage time, questioning the long-term stability of wide-gap ACIGS solar cells. Furthermore, the efficiency of samples with very high Ga and Ag contents depends on the voltage sweep direction. It is proposed that the hysteresis behavior is caused by a redistribution of mobile Na ions in the 1:1:2 absorber lattice upon voltage bias. Finally, a broader perspective on OVC formation in the ACIGS system is provided and fundamental limitations for wide-gap ACIGS solar cells are discussed.

1. Introduction

The optimum bandgap energies (E_G) of solar absorbers in a 2-terminal (4-terminal) photovoltaic tandem device are 0.94 eV (0.95 eV) for the bottom and 1.61 eV (1.74 eV) for the top cell.^[1] In the (Ag,Cu)(In,Ga)Se₂ (ACIGS) material system, a minimum E_G of about 1.0 eV is reached for (Ag,Cu)InSe₂ with $[\text{Ag}]/[\text{I}] < 0.25$ ($[\text{I}] = [\text{Ag}] + [\text{Cu}]$) and a maximum value of $\approx 1.8\text{ eV}$ is obtained for the ternary AgGaSe₂ compound.^[2,3]

Dr. J. Keller, Prof. L. Stolt, Dr. K. V. Sopiha, Dr. J. K. Larsen, Dr. L. Riekehr, Prof. M. Edoff
 Ångström Solar Center
 Division of Solar Cell Technology
 Uppsala University
 75121 Uppsala, Sweden
 E-mail: jan.keller@angstrom.uu.se

 The ORCID identification number(s) for the author(s) of this article can be found under <https://doi.org/10.1002/solr.202000508>.

© 2020 The Authors. Published by Wiley-VCH GmbH. This is an open access article under the terms of the Creative Commons Attribution License, which permits use, distribution and reproduction in any medium, provided the original work is properly cited.

DOI: 10.1002/solr.202000508

Thus, ACIGS is a promising absorber candidate for bottom and top cells. For a pure chalcopyrite-based tandem device, an almost perfect match is the combination of CuInSe₂ ($E_G = 1.04\text{ eV}$) and CuGaSe₂ ($E_G = 1.68\text{ eV}$).^[4] In the case of low-gap absorbers with pure CuInSe₂ surface regions, efficiencies (η) of $\eta \geq 18\%$ are reported and further progress is expected.^[5,6] However, to this date, the efficiency of CuGaSe₂-based solar cells is still limited to $\eta < 12\%$.^[7] The most pronounced loss, as compared with absorbers with $[\text{Ga}]/[\text{III}] < 0.4$ ($[\text{III}] = [\text{Ga}] + [\text{In}]$), is the significantly increased deficit in open-circuit voltage (V_{OC}) with respect to the bandgap energy.^[8] For commonly applied CdS buffer layers, and in the absence of an ordered vacancy compound (OVC) at the absorber surface,^[9,10] a negative conduction band offset (CBO), a so-called cliff, is predicted at the buffer/CuGaSe₂ interface.^[4] The resulting reduction in type inversion increases the interface recombination rate, thereby limiting V_{OC} .^[11] Alternatively, an increased bulk recombination 1) via deep Ga_{Cu} anti-site defects,^[12–15] 2) via deep acceptors,^[16,17] or 3) at Cu-enriched grain boundaries^[18] is suggested as a reason for the relatively poor performance of CuGaSe₂ solar cells. Nevertheless, the fact that the highest V_{OC} of $\approx 1\text{ V}$ was achieved by using an alternative Zn_{1-x}Sn_xO_y (ZTO) buffer layer (resulting in a positive CBO [i.e., “spike”]) signifies the dominance of recombination at the CdS/CuGaSe₂ interface.^[7,19] However, it cannot be excluded that the bulk properties of CuGaSe₂ are inferior to low-gap absorbers, too.

A possible way to decrease recombination at the interface between a CdS buffer and a wide-gap chalcopyrite absorber is to optimize the CBO by adjusting the level of Ag alloying in ACIGS. Calculations within density functional theory (DFT) predict a positive CBO with ACIGS bandgaps $> 1.6\text{ eV}$ for the compositional range of roughly $[\text{Ag}]/[\text{I}]$ and $[\text{Ga}]/[\text{III}] > 0.75$.^[2] Several promising results, with V_{OC} values of $890\text{ mV} \leq V_{OC} \leq 960\text{ mV}$ and efficiencies of $13\% \geq \eta \geq 9.3\%$, were reported for A(C)IGS solar cells with $1.6\text{ eV} \leq E_G \leq 1.75\text{ eV}$.^[20–22] However, these efficiencies are still too low to consider wide-gap ACIGS as a practical top cell absorber material.

In a recent study, we investigated the solar cell performance in the ACIGS compositional range of $0.2 \leq [\text{Ag}]/[\text{I}] \leq 0.8$ for two different $[\text{Ga}]/[\text{III}]$ ratios of 0.72 and 0.85, resulting in

$E_G = 1.45\text{--}1.61\text{ eV}$.^[2] The standard CdS buffer layer was compared with an alternative ZTO buffer, leading to consistently higher V_{OC} values for ZTO. This indicates that even for optimized CBO values (CBO = 0–0.3 eV), interface recombination still plays a role. The results for samples with $[Ag]/[I] \leq 0.5$ confirmed the predictions from DFT: a significantly lower V_{OC} was measured for samples with an expected negative (or very low) CBO at the buffer/ACIGS interface. However, for the sample with the highest Ag ($[Ag]/[I] = 0.8$) and Ga ($[Ga]/[III] = 0.85$) content, the V_{OC} deficit increased again, despite a clear spike configuration at the CdS/ACIGS interface was calculated in this case. In addition, a distinct distortion in current–voltage (I – V) characteristics was observed. This is particularly unfortunate because this sample exhibits an almost optimum E_G for 2-terminal tandem top cells of 1.61 eV. Large (Ag,Cu)(In,Ga)₃Se₅ OVC (1:3:5) patches were detected at the front and back contact, which are believed to be responsible for the performance deterioration of the corresponding solar cells. A significantly reduced tolerance to off-stoichiometry for ACIGS films with simultaneously high Ag and Ga concentrations was suggested to explain the substantial formation of 1:3:5 compounds.^[2] In addition, a miscibility gap was predicted for high Ag and intermediate Ga contents.^[23]

The present contribution first reinvestigates the solar cell performance of the samples with a CdS buffer from our previous work^[2] after ≈ 8 months of air exposure (“office storage”) and links the observed differences in long-term stability to the formation of OVCs. In the second and third part of the article, the effect of a varied off-stoichiometry and the corresponding tendency to OVC formation are investigated for samples with a constant absorber composition of $[Ag]/[I] = 0.8$ and $[Ga]/[III] = 0.85$ (i.e., same as in the previous study^[2]). This composition is chosen because the resulting E_G is in the optimum range for top cells, as mentioned earlier. The final part provides a general discussion about the formation of OVCs in the entire

composition range of the ACIGS system, connecting their occurrence with the varying tolerance to off-stoichiometry for different absorber compositions.

2. Results and Discussion

2.1. Effect of ACIGS Composition on Performance Degradation

Figure 1 shows the I – V results of the best solar cells for different $[Ag]/[I]$ and $[Ga]/[III]$ ratios in ACIGS from our previous work,^[2] as measured 3 days and ≈ 8 months after completion. The corresponding bandgaps, initial V_{OC} values, and $[I]/[III]$ ratios are provided as well. The E_G values were extracted from external quantum efficiency spectra (inflection point method^[24]), as it is the case throughout this article. The results correspond approximately to the surface bandgap because a small $[Ga]/[III]$ depth gradient is present for all samples (for more details, we refer to ref. [2]). Apart from a slightly increased series resistance, no significant degradation is observed for samples with $[Ag]/[I] = 0.2\text{--}0.5$, independent of the Ga content. The sample with the lowest Ag and Ga levels even showed a significant V_{OC} improvement after ≈ 8 months (+65 mV), which is not understood at this point, but a similar effect of long-term storage in air was reported before.^[6]

However, the samples with $[Ag]/[I] = 0.8$ show a clear drop in efficiency after ≈ 8 months. The distinct kink in the I – V curves, leading to fill factor (FF) losses, indicates the presence of a transport barrier for the diode- and photocurrent that evolved/increased over time. Presumably, the same type of barrier already limited the initial performance of the sample with $[Ga]/[III] = 0.85$, but was initially absent for $[Ga]/[III] = 0.72$. As aforementioned, large patches of OVCs were detected at the interfaces for the sample with $[Ga]/[III] = 0.85$, which were

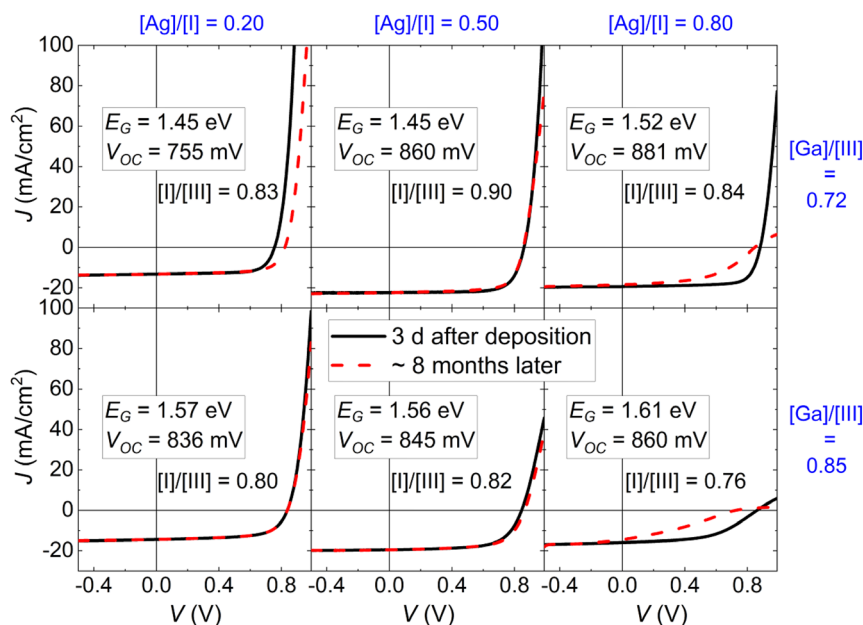


Figure 1. I – V characteristics under illumination of the samples investigated in ref. [2], measured 3 days (black solid lines) and ≈ 8 months after cell completion (red dashed lines). The initial V_{OC} values and corresponding absorber bandgaps are given as well.

suggested to be the origin of the I - V distortion observed already shortly after cell completion.^[2] However, the discovery of the evolving transport barrier for the sample with $[Ga]/[III] = 0.72$ motivates a closer and more integral investigation of the OVC formation in all the samples from Figure 1. This was done by using Raman spectroscopy on the completed devices after ≈ 8 months. A green laser ($\lambda = 532$ nm) was used, resulting in a probing depth of about 200 nm into the absorber. The results are shown in Figure 2.

For wavenumbers (k) of $k \approx 180$ cm^{-1} (A_1 mode) and $k \approx 270$ cm^{-1} (presumably $B_2 + E$ modes^[25,26]), peaks from the intended (Ag,Cu)(In,Ga)Se₂ (1:1:2) phase are visible for all samples. In general, the absorber-related peaks are shifted to higher k -values for higher Ga concentrations and lower k -values for larger Ag contents. The peaks at $k \approx 300$ cm^{-1} stem from the CdS layer, and the ratio between the CdS and the absorber signals varies somewhat laterally. Both samples with $[Ag]/[I] = 0.8$

show a very pronounced signal from OVCs at the absorber surface. The sample with $[Ag]/[I] = 0.5$ and $[Ga]/[III] = 0.85$ also exhibits a small OVC peak, while for all other samples no OVC is detected. These OVCs are proposed to be 1:3:5 and not 1:5:8 compounds, as confirmed by energy-dispersive X-ray spectroscopy (EDS) measurements in scanning transmission electron microscopy (STEM), which are presented and discussed later in the article.

The Raman results suggest that the presence of OVCs is linked (directly or indirectly) to the deterioration and instability in device performance. However, it is not clear why the sample with $[Ag]/[I] = 0.8$ and $[Ga]/[III] = 0.72$ did not show the corresponding transport barrier from the very beginning. According to the OVC/1:1:2 peak ratios, the volume fraction of OVCs at the absorber surface should be at least comparable for both samples with $[Ag]/[I] = 0.8$. A possible explanation is that OVCs at the back contact, which may be more pronounced for the $[Ga]/[III] = 0.85$ sample (not detectable by Raman on the front surface), are responsible for the kink in I - V . The evolving current blocking may then be caused by Na redistribution/in-diffusion at room temperature, which depends on the extent of OVCs at the back. Further evidence for a correlation of OVCs at the back, their accumulation of Na and the formation of a transport barrier is provided later in the text. Extensive formation or growth of OVCs at room temperature can be ruled out though. This was confirmed by reinvestigating a TEM lamella ($[Ag]/[I] = 0.8$ and $[Ga]/[III] = 0.85$) after ≈ 8 months, which did not show any migration of phase/grain boundaries of the OVCs (not shown here).

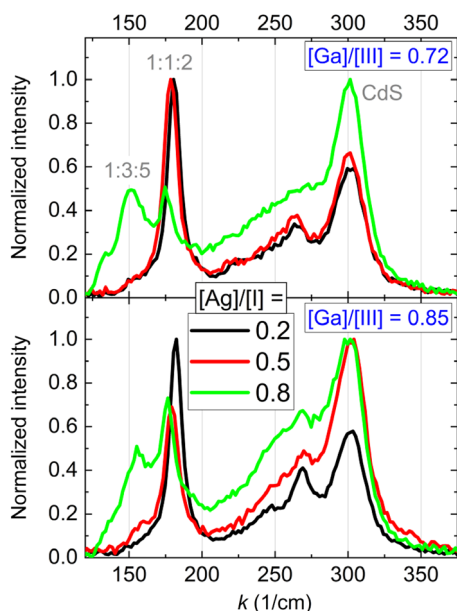


Figure 2. Raman spectra measured after ≈ 8 months on the same samples (completed cells) as in Figure 1. The probing depth into the absorber is about 200 nm.

2.2. ACIGS Stoichiometry: Impact on Solar Cells with $E_G > 1.6$ eV

The results presented earlier indicate a significantly increased tendency to OVC formation for compositions of $[Ag]/[I] > 0.5$ and $[Ga]/[III] \geq 0.72$. To explore the effect of absorber (off-)stoichiometry on the solar cell performance and OVC formation in more detail, five additional samples, spanning a range of $0.76 \leq [I]/[III] \leq 1.06$, were processed with the same cation ratios of $[Ag]/[I] = 0.8$ and $[Ga]/[III] = 0.85$ as in ref. [2]. These samples were characterized within 3 days after absorber deposition, but no long-term stability tests were conducted. The results are shown in Figure 3 and summarized in Table 1. Figure 3a

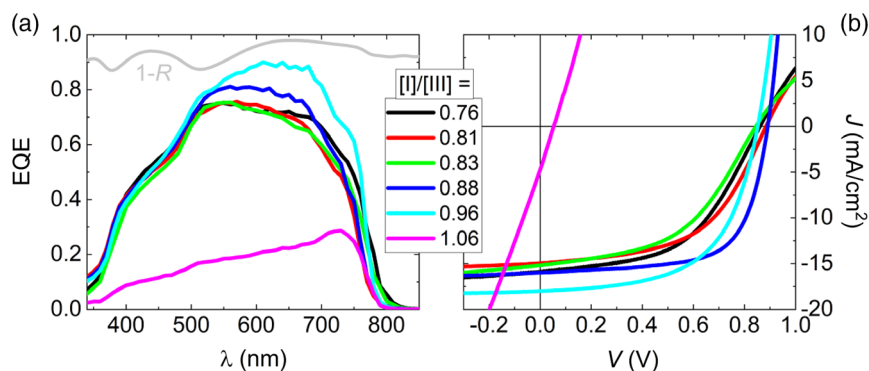


Figure 3. a) EQE spectra and b) corresponding I - V characteristics under illumination of the best solar cells with different $[I]/[III]$ ratios and constant $[Ag]/[I] = 0.8$ and $[Ga]/[III] = 0.85$. All samples were measured within 3 days after absorber deposition.

Table 1. Device parameters and absorber bandgap energies of the best solar cells with different [I]/[III] ratios but constant [Ag]/[I] = 0.8 and [Ga]/[III] = 0.85 (see Figure 3). The numbers in parentheses are extracted from reverse I - V sweeps, while all other values are determined from forward sweeps.

[I]/[III]	E_G [eV]	$J_{SC,EQE}$ [mA cm ⁻²]	V_{OC} [mV]	FF [%]	η [%]
0.76	1.61	15.9	860	51.5	7.0
0.81	1.63	15.0	884	53.4	7.1
0.83	1.62	15.2	845	48.9	6.3
0.88	1.63	16.0	891 (910)	66.8 (70.2)	9.5 (10.2)
0.96	1.62	18.0	852 (859)	58.3 (62.9)	9.0 (9.7)
1.06	1.62	4.8	53	25.3	0.1

shows the external quantum efficiency (EQE) spectra for the best cell of each sample and the reflection loss ($1-R$) for the sample with [I]/[III] = 1.06 (R is similar for all samples). The extracted bandgap values are added in Table 1. Small changes in E_G are due to marginally varying [Ag]/[I] and [Ga]/[III] ratios for the samples (see Section 4).

For the [I]-rich sample, a very low EQE is measured and the corresponding I - V curve in Figure 3b indicates strong shunting issues. Still, a weak diode-like characteristic is seen for this sample, too (see Figure S1, Supporting Information). No $Cu_{2-x}Se$ or $Ag_{2-x}Se$ phases, which could potentially act as shunt paths,^[27] were found in Raman measurements (not shown here). In the ternary Ag-Ga-Se system, formation of Ag_9GaSe_6 instead of $Ag_{2-x}Se$ is expected for [I]/[III] > 1.^[28] Thus, the results indicate that a similar I_9 -III-Se₆ (photo-)conductive compound forms here instead and causes severe shunting. Indeed, top-view EDS analysis in scanning electron microscopy (SEM) confirmed the presence of purely ternary Ag_9GaSe_6 grains located mainly in the upper part of the [I]-rich absorber and homogeneously distributed laterally (Figure S2 and S3, Supporting Information). The existence of this low- E_G ($E_G \approx 0.56$ eV^[29]), nonphotoactive phase increases the parasitic absorption in the absorber and may explain the increasing EQE with wavelength (λ) for this sample.

The highest EQE is measured for a near-stoichiometric composition of [I]/[III] = 0.96, but collection losses are evident for this sample, too (see Figure S4, Supporting Information).

Accordingly, this sample shows by far the highest short-circuit current density ($J_{SC,EQE}$), as deduced from the corresponding EQE measurement. Nevertheless, the FF is quite low, which is suggested to originate from remaining secondary phases in the film. In fact, some widely dispersed Ag_9GaSe_6 grains were found by top-view SEM + EDS even for the [I]/[III] = 0.96 sample, in regions where the film shows pin holes/openings (not shown here). For the [I]/[III] = 0.88 sample, a reduced EQE level is measured, which is ascribed to the presence of OVCs at the heterojunction, as discussed in the next section. No Ag_9GaSe_6 was detected here. This sample shows the highest FF, V_{OC} , and η of all solar cells with a constant absorber composition of [Ag]/[I] = 0.8 and [Ga]/[III] = 0.85. Like for the near-stoichiometric sample, no distortion/kink is observed for [I]/[III] = 0.88. All other samples with [I]/[III] ≤ 0.83 share the same undesired features. They show a similarly low EQE maximum of ≈0.8 and exhibit a strong kink in I - V , expressed as low FF and $J_{SC,EQE}$ values. It is proposed that the losses in $J_{SC,EQE}$ are mainly caused by OVCs at the heterojunction, while the FF losses originate from the OVCs at the back contact. This hypothesis is supported by the results in the next section. Additional solar cells with the same [Ag]/[I] and [Ga]/[III] were fabricated and the repeated characterization (not shown here) confirmed the observed trends in EQE (i.e., higher EQE top level when approaching stoichiometry). Overall, the optoelectrical characterization clearly illustrates the importance of stoichiometry in ACIGS solar cells with $E_G > 1.6$ eV. The results identify a narrow “sweet-spot” region for a ratio of $0.88 < [I]/[III] < 0.96$, at least for the absorber composition and three-stage process applied in this study.

Interestingly, the solar cells with [I]/[III] = 0.88 and 0.96 showed a strong hysteresis effect in I - V measurements. Figure 4 shows the corresponding characteristics for forward and reverse sweeps. Both samples exhibit a substantial gain in FF for a reverse voltage sweep (V from +1 V to -0.5 V), while the sample with [I]/[III] = 0.88 also shows a 19 mV increase in V_{OC} . This effect is highly reproducible and the same curves were measured for several consecutive sweep cycles. The corresponding efficiencies are increased by 0.7% absolute (see Table 1), leading to a top efficiency of 10.2% at $E_G = 1.63$ eV, without antireflective coating (ARC). This value is in the range of the best efficiencies reported for chalcopyrite solar cells with a similar E_G .^[20,30–32] The highest V_{OC} of 910 mV still only reaches ≈68% of the theoretical

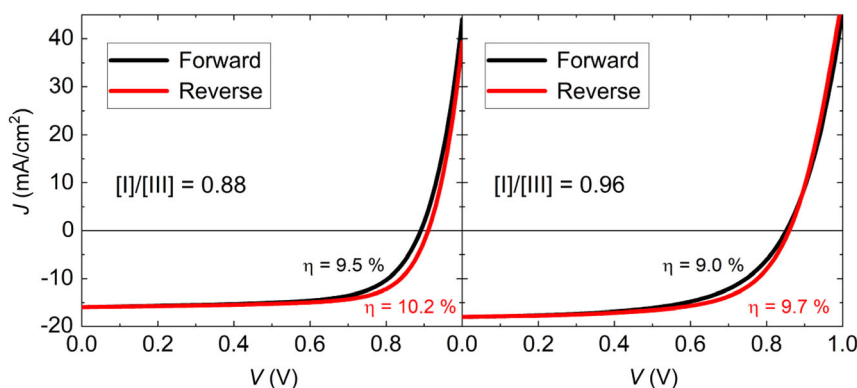


Figure 4. I - V characteristics under illumination for the best cells with [I]/[III] = 0.88 and 0.96 ([Ag]/[I] = 0.8 and [Ga]/[III] = 0.85) measured under forward and reverse voltage sweeps. The sweep range is $V = -0.5$ V \leftrightarrow +1.0 V.

Shockley–Queisser limit, while for the best low-gap cells with CdS buffers values $> 85\%$ are achieved.^[33] Thus, although a positive CBO is predicted for this sample composition, a high non-radiative recombination rate at the heterojunction and/or in the bulk remains. For the samples with $[I]/[III] \leq 0.83$, a small hysteresis but no significant improvement was observed by reverse sweeping and the kink did not disappear. A possible reason may be that the observed transport barrier interferes with the mechanism responsible for the hysteresis. After identification of the hysteresis effect, the other samples from Figure 1 with $[Ag]/[I] \leq 0.5$ were tested as well. However, no dependence on sweep direction was observed here. This indicates that free charge carrier transport is affected by an applied voltage bias for samples with $[Ag]/[I] = 0.8$.

A possible explanation for the hysteresis effect may be the presence of mobile ions causing space-charge polarization of the absorber by their redistribution upon voltage bias. The corresponding charge accumulation would introduce spatial variations in the space-charge region width, thereby influencing carrier collection and transport. Similar polarization effects caused by high mobility of anions are reported to affect I – V characteristics of perovskite-based solar cells.^[34] A possible candidate in the present absorber films are Na^+ ions, which have a high diffusion coefficient in grain boundaries and in the bulk.^[35,36] Even faster diffusion can be expected through ordered arrays of vacancies in the OVCs. Faster diffusion indicates that also the drift upon voltage bias is facilitated. As shown in Figure 2, a major OVC formation at the absorber surface is only found for samples with $[Ag]/[I] = 0.8$, which also show the pronounced hysteresis effect. This points to a correlation between OVCs and the hysteresis, but the mechanism relies on the assumption that 1) Na preferably populates the OVC patches and that 2) OVCs are also found for near-stoichiometric absorbers ($[I]/[III] = 0.96$). This hypothesis is further examined in the next section.

2.3. ACIGS Stoichiometry: Impact on OVC Formation

The solar cell characteristics presented in the previous section highlight the crucial role of the absorber stoichiometry for ACIGS with high Ag contents. In this section, the OVC formation of the same samples with $[Ag]/[I] = 0.8$ and $[Ga]/[III] = 0.85$

is illustrated and quantified in dependence of the integral stoichiometry.

Figure 5a shows the Raman spectra of the corresponding solar cells, zoomed into the region of the main 1:1:2 ACIGS and 1:3:5 OVC peaks. The 1:3:5 peak is relatively broad because it consists of overlapping signals from Ga- and In-enriched OVCs, as discussed later. In addition to the 1:3:5 signature, a second peak/shoulder at $k \approx 140 \text{ cm}^{-1}$ is visible for most samples, which may be ascribed to a different 1:3:5 mode or could indicate the parallel presence of 1:5:8 OVCs, as seen for very [I]-poor $CuGaSe_2$.^[38] It is obvious that the highest OVC fraction at the surface occurs for the samples with $[I]/[III] \leq 0.83$. This correlates well with the reduced EQE level and the strong kink in I – V for these samples, which further suggests the detrimental role of an extensive OVC formation at the surface. For $[I]/[III] = 0.88$, a slightly lower but still significant OVC signal is measured. The near-stoichiometric sample ($[I]/[III] = 0.96$) shows a minor OVC peak, which is only marginally larger than the signal for the [I]-rich sample. For the latter one, it is not clear if the weak shoulder at $k \approx 160 \text{ cm}^{-1}$ stems from remaining OVCs or can be ascribed to an unknown background signal (more likely). In Figure 5b, the peak intensities of the OVCs are normalized to the OVC + 1:1:2 intensities for the different $[I]/[III]$ ratios. It is not understood at this stage why the OVC fraction at the front surface seems to saturate for $[I]/[III] \leq 0.83$. A possible explanation is that the OVC depth extension starts to exceed the Raman probing depth for lower $[I]/[III]$ values. Raman was also measured on the back side of the samples, after selectively peeling off the absorbers (see Figure S5, Supporting Information). Significant OVC formation is found at the back for $[I]/[III] \leq 0.83$, while no OVCs are detected for $[I]/[III] \geq 0.88$. Notably, the by far largest OVC signal from the back side was measured for $[I]/[III] = 0.81$, which is not understood but becomes important later.

In our earlier work,^[37] we performed the same Raman analysis (identical settings) on $Cu(In,Ga)Se_2$ (CIGS) absorbers with Ga-free surfaces (also three-stage coevaporation process). The results are added in Figure 5b for comparison. It is obvious that the Ag- and Ga-rich absorbers are more susceptible to OVC formation, which indicates less tolerance to off-stoichiometry. This topic is addressed in more detail in the final section of this article.

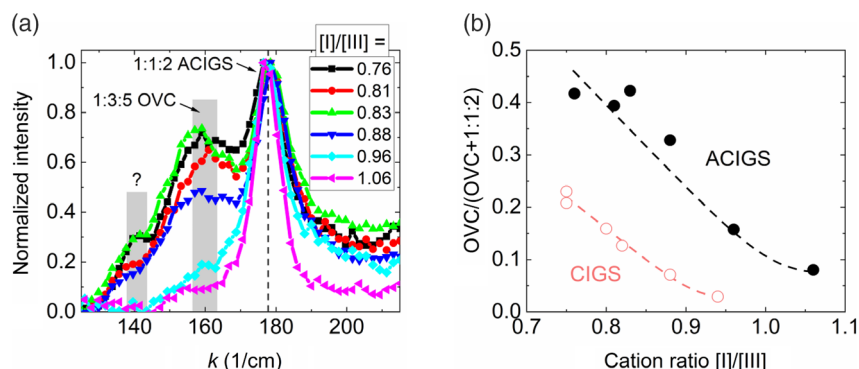


Figure 5. a) Raman spectra of solar cell samples with different $[I]/[III]$ ratios and constant $[Ag]/[I] = 0.8$ and $[Ga]/[III] = 0.85$, normalized to the 1:1:2 ACIGS peak intensity. b) Corresponding OVC peak intensities normalized to (OVC + 1:1:2) intensities. Data extracted from Raman measurements on $Cu(In,Ga)Se_2$ (CIGS) with varying off-stoichiometry and constant $[Ga]/[III] = 0.18$ (pure $CuInSe_2$ at surface) from ref. [37] is added for comparison.

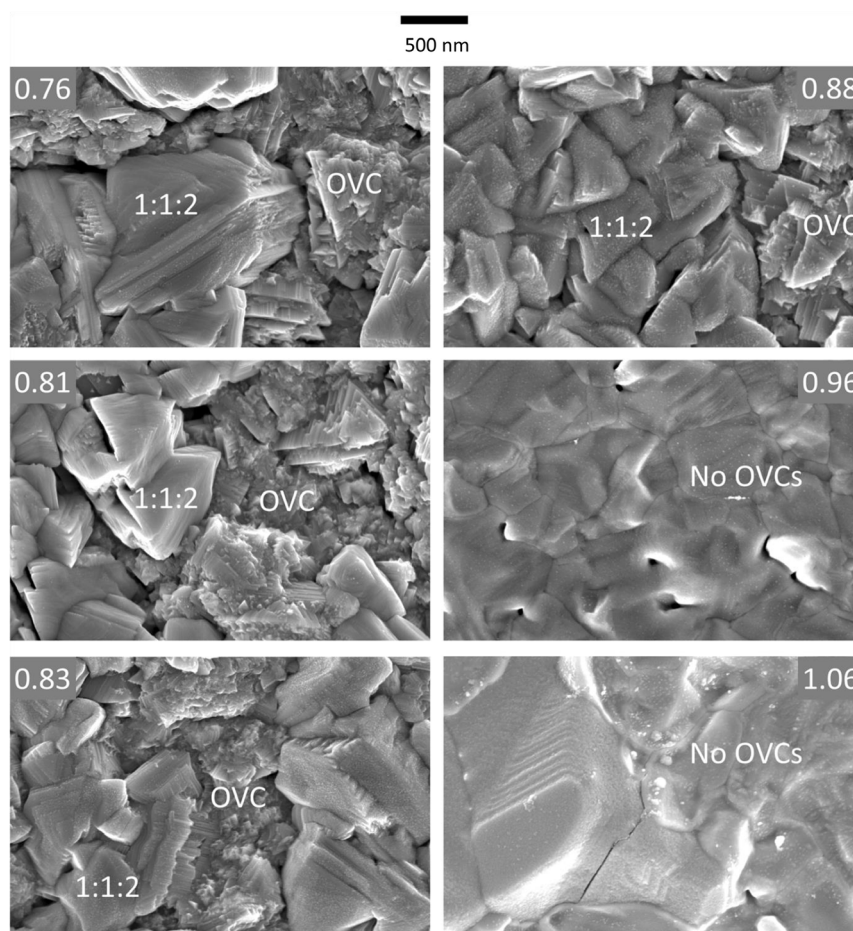


Figure 6. Top-view SEM images of the bare absorber surfaces with different $[I]/[III]$ ratios and constant $[Ag]/[I] = 0.8$ and $[Ga]/[III] = 0.85$.

To estimate the lateral distribution and extension of the OVCs in dependence of the stoichiometry, SEM and EDS top-view analyses were conducted on the bare absorber layers. The corresponding SEM images are shown in **Figure 6**. For $[I]/[III] \leq 0.88$, a two-phase microstructure, consisting of rather smooth 1:1:2 grains and finer structured OVCs, is visible. The phase assignment by EDS analysis is exemplified for $[I]/[III] = 0.83$ in Figure S6, Supporting Information. As expected from the Raman results (probed area similar to presented SEM sections), the OVC volume fraction is decreasing toward stoichiometric absorber composition. Furthermore, a smoother and more compact surface is observed for $[I]/[III] = 0.96$ and 1.06. No clear trend in grain size of the 1:1:2 phase is detected.

To reveal the OVC depth distribution and to obtain accurate chemical quantification, cross-sectional STEM-EDS was conducted on the samples with $[I]/[III] = 0.76$, 0.88, and 0.96. The quantified elemental and $[I]/[III]_{\text{EDS}}$ maps are shown in **Figure 7**.

For the largest off-stoichiometry, extensive OVC patches are detected at the front and back contact, but not in the middle of the absorber. This is suggested to be a consequence of the three-stage process (I)-poor evaporation rates in the beginning and at the end). Unpublished results from ongoing work indicate that the OVC patches are rather homogeneously distributed when

applying a one-stage process. The detected OVCs show a strong reduction in Ag content and are either Ga- or In-enriched. The latter ones are smaller on average and occur only at the front surface, where both configurations approximately alternate. Only Ga-enriched OVCs are present at the back contact. The total OVC volume fraction is about 13% for this sample. Thus, a low collection efficiency in the OVCs or trapping of charge carriers by a large CBO at the OVC/1:1:2 and CdS/OVC interfaces may explain the observed losses in $J_{\text{SC, EQE}}$ for the [I]-poor samples.^[4,19,39–41] Indeed, OVCs are generally supposed to exhibit lower conduction band and valence band edges than the corresponding 1:1:2 phase, potentially creating an electron transport barrier for electrons captured in the OVCs.^[42] The average $[I]/[III]_{\text{EDS}}$ ratios are 0.39 ± 0.03 in the Ga-enriched and 0.39 ± 0.02 in the In-enriched OVC regions. This number is considerably closer to the theoretical value for a 1:3:5 ($[I]/[III] = 0.33$) as compared with that for a 1:5:8 compound ($[I]/[III] = 0.2$). The slightly overestimated $[I]/[III]_{\text{EDS}}$ ratio may be explained by the extension/thickness of the TEM lamella and morphology of the OVCs. However, the presence of some minor 1:5:8 OVCs cannot be ruled out (see second OVC peak in Raman; Figure 5). Outside the OVC regions, the bulk shows almost perfect 1:1:2 stoichiometry, reaffirming the very narrow single-phase region of the $\text{Ag}_{0.8}\text{Cu}_{0.2}\text{In}_{0.15}\text{Ga}_{0.85}\text{Se}_2$ alloy.

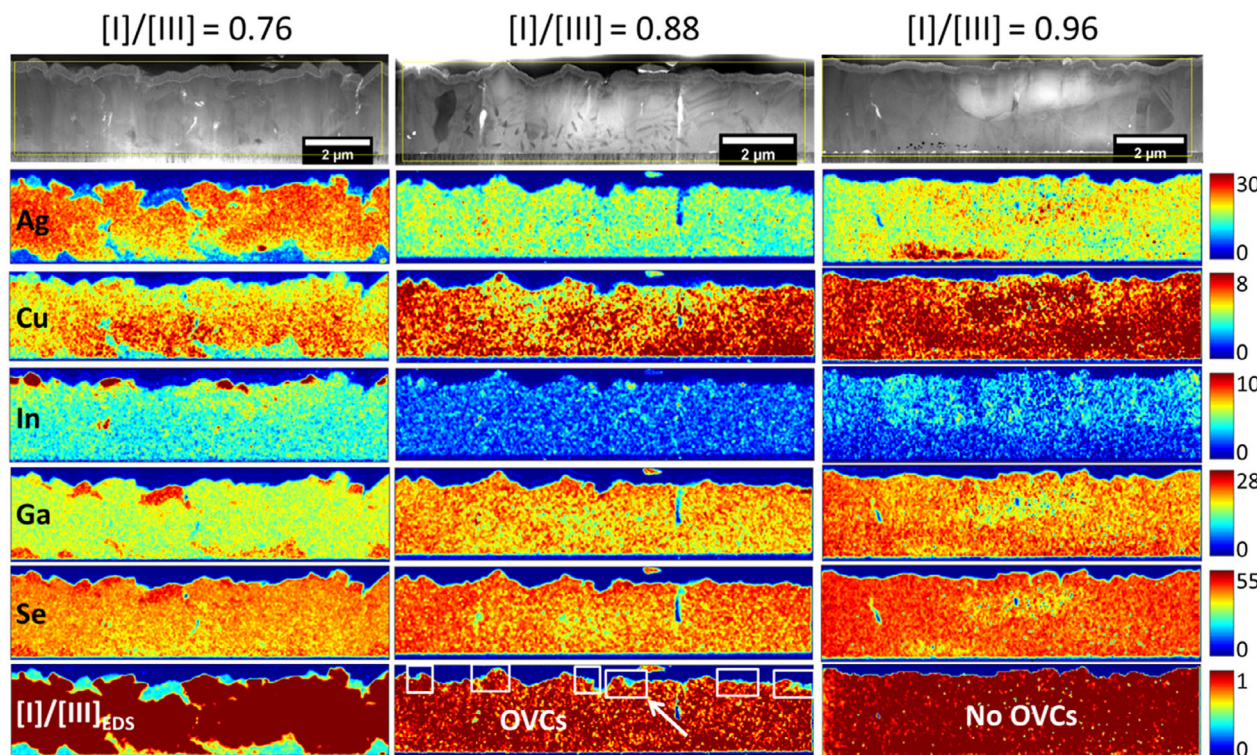


Figure 7. STEM bright-field images and quantified elemental (in at%) as well as $[I]/[III]_{EDS}$ maps of the samples with $[I]/[III] = 0.76$, 0.88 , and 0.96 and constant $[Ag]/[I] = 0.8$ and $[Ga]/[III] = 0.85$, as extracted from EDS analysis. The color bars show the concentrations in at% and the quantified $[I]/[III]_{EDS}$ ratios. The white arrow marks the OVC patch investigated in more detail in Figure 8. The Ag-enrichment at the back for $[I]/[III] = 0.96$ is due to Ag droplet formation under electron beam exposure during EDS mapping.

Table 2. Cation ratios $[Ag]/[I]_{EDS}$ and $[Ga]/[III]_{EDS}$ inside the OVC regions of the sample with $[I]/[III] = 0.76$ (average $[Ag]/[I] = 0.8$ and $[Ga]/[III] = 0.85$) as extracted from STEM-EDS (see Figure 7). The errors are standard deviations.

Parameter	OVC region	In-enriched	Ga-enriched
$[Ag]/[I]_{EDS}$	Front	0.71 ± 0.06	0.60 ± 0.06
	Back	–	0.61 ± 0.06
$[Ga]/[III]_{EDS}$	Front	0.58 ± 0.01	0.83 ± 0.02
	Back	–	0.84 ± 0.01

Table 2 shows the OVC cation ratios averaged over all detected patches. It is obvious that the composition of the Ga-enriched patches is identical at the back and front contacts. These OVCs have a similar $[Ga]/[III]$ as the 1:1:2 phase, but show a greater reduction in $[Ag]/[I]$ as compared with the In-enriched ones, which have a considerably decreased $[Ga]/[III]$ value instead. The coexistence of two compositions of 1:3:5 phase can either be caused by 1) a miscibility gap in the OVC phase itself or 2) not reaching thermodynamic equilibrium within the absorber volume deposited in the third stage (because it had the least time to equilibrate). The miscibility gap would be more likely if a continuous interface between Ga- and In-enriched OVC grains would have been observed. Such configuration was never present within the analyzed lamellae, rendering the “non-equilibrium” scenario more probable. This conclusion gives hope that at least some of the

OVC patches at the front can be eliminated by modifying the deposition protocols and/or additional heat treatment. In contrast, the difference of the $[Ag]/[I]$ cation ratios in the Ga-enriched OVCs and the 1:1:2 phase seems to have a thermodynamic origin because the values are consistent and independent on the grain location. A preliminary DFT study of OVC thermodynamics was conducted and it supports the aforementioned claims. More details will be presented in a separate publication shortly.

To estimate the bandgaps of these OVCs, the E_G values of the ternary 1:3:5 compounds need to be considered first. For $CuIn_3Se_5$ and $CuGa_3Se_5$, values of $E_G \approx 1.23$ eV^[43] and ≈ 1.85 eV^[43,44] are reported, respectively. The existence of a $AgIn_3Se_5$ compound is inconclusive,^[45–47] but a bandgap of ≈ 1.72 eV was measured for nanoparticles with suggested $AgIn_3Se_5$ stoichiometry.^[45,46] No 1:3:5 compound was detected in the Ag–Ga–Se system, but for the existing $AgGa_3Se_5$ a bandgap of ≈ 2.1 eV is reported.^[48] As E_G is generally slightly higher (≈ 0.1 eV) for the 1:3:5 than for the 1:5:8 OVCs in the other ternary systems, a value of $E_G = 2.2$ eV is assumed for a “fictive” $AgGa_3Se_5$ compound. A 2D linear interpolation (see Figure S7, Supporting Information) leads to bandgaps of 1.96 eV for the Ga-enriched and 1.87 eV for In-enriched OVCs. This rough estimation indicates that the bandgap of the OVCs is considerably larger than that of the 1:1:2 ACIGS bulk material, suggesting that the EQE losses for the [I]-poor samples are rather due to free carrier capture and trapping and not (only) parasitic absorption. If the collection efficiency of electrons generated in

OVCs was much lower than for charge carriers generated in the 1:1:2 region, a kink/shoulder at the OVC bandgap ($\lambda \approx 650$ nm) would be expected in the corresponding EQE spectra.

In agreement with the Raman measurements on the absorber back side (Figure S5, Supporting Information), the $[I]/[III] = 0.88$ sample does not show any OVCs at the back contact. Instead, rather small (maximum extension ≈ 200 nm), either Ga- or In-enriched, OVC patches are detected at the front contact. This is in line with the distinct surface OVC signal in Raman (see Figure 5). The total OVC volume fraction is reduced to 1.6%. Still, because all of the OVCs are located in the region where the majority of charge carriers are generated, an impact on solar cell performance is expected. Indeed, significant collection losses are observed in EQE for this sample (Figure 3a), which indicates that OVCs at the front contact are generally responsible for the reduced $J_{SC,EQE}$ values of samples with [I]-poor absorber composition. In contrast, the $[I]/[III] = 0.88$ sample does not show any kink and exhibits the highest FF. It is therefore suggested that the distortion in I - V for $[I]/[III] \leq 0.83$ is caused either directly or indirectly by OVCs at the back contact. The exact mechanism behind the impeded charge carrier transport (or extraction/injection) needs further investigation. According to Figure 7, it seems that also regions with a direct 1:1:2/back contact interface are present for $[I]/[III] = 0.76$, which should locally allow for an unhindered charge transfer. Thus, at this point it is not clear if the responsible transport barrier is solely located at the interface between the large OVC patches and the back contact or if, for instance, a very thin OVC (< 10 nm) covers the entire back contact. Alternatively, Na accumulation in the back OVCs may result in the absence of Na at the direct 1:1:2/MoSe₂ interface, where it is supposed to reduce the barrier height for hole extraction.^[49,50]

Figure 8 shows a magnified STEM image and the corresponding elemental mappings of a region containing an In-enriched

OVC. The position is indicated by a white arrow in Figure 7. A sharp OVC/1:1:2 phase boundary, where the composition changes abruptly, is evident. Interestingly, a slight radial Cu increase and Ag decrease on the periphery of the OVC is found. This feature resembles a diffusion profile with a discontinuity at the interface, indicating that the system is not in thermodynamic equilibrium and elemental redistributions may proceed further during postdeposition treatments or storage. The included graph shows an elemental line scan across the CdS/OVC/1:1:2 interfaces following the direction of the white arrow in the STEM image. The corresponding $[I]/[III]_{EDS}$ profile confirms a 1:3:5 stoichiometry of the OVC (see Figure S8, Supporting Information), which is in contrast to earlier studies where a 1:5:8 stoichiometry is claimed for similar absorber compositions.^[26,51,52]

The near-stoichiometric TEM sample ($[I]/[III] = 0.96$) in Figure 7 does not contain any OVC patches. This is in line with the very small OVC signal in Raman and the SEM analysis and indicates that the few existing OVCs are widely dispersed at the absorber surface (see also Figure S9, Supporting Information). Also, no other secondary phases, like the suspected Ag₃GaSe₆, are found in the small absorber volume extracted by the TEM lamella. This does not rule out their existence, but suggests a very small volume fraction and/or wide dispersion. The seemingly Ag-enriched region at the back contact of this sample is an artifact and originates from Ag precipitations (droplets), which formed during electron beam irradiation (STEM image taken before EDS mapping). For the other samples no such artifact was observed.

The presented microstructural and chemical investigations provide a comprehensive picture of the relationship between stoichiometry and OVC formation. It was suggested earlier that the evolving transport barrier for the samples with $[Ag]/[I] = 0.8$ is a result of Na diffusion processes at room temperature, triggered, or at least affected, by the presence of OVCs at the back contact.

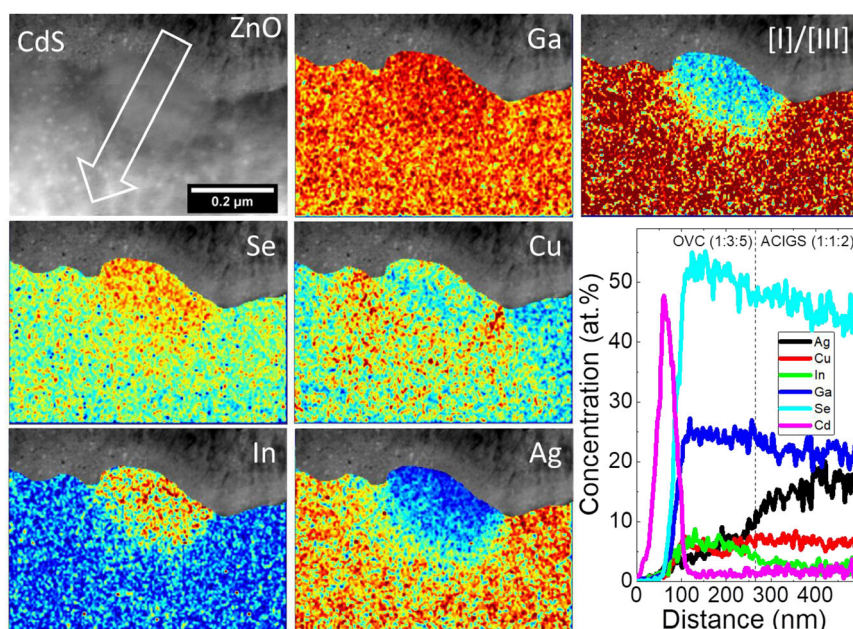


Figure 8. Magnified STEM bright-field image of the sample with $[I]/[III] = 0.88$ ($[Ag]/[I] = 0.8$ and $[Ga]/[III] = 0.85$) and corresponding elemental and $[I]/[III]_{EDS}$ maps deduced from STEM-EDS. The analyzed region is indicated by a white arrow in Figure 7. The graph in the lower right corner shows an elemental line scan across the CdS/1:3:5/1:1:2 interfaces, as displayed by the white arrow in the STEM image.

In addition, it was speculated that the observed I - V hysteresis may be a result of Na migration or displacement inside the OVCs during voltage sweep.

The identified spatial OVC distribution allows verifying Na accumulation in the OVC patches. In this case, the Na concentration in the upper absorber region is expected to correlate with the OVC signal in Raman, i.e., a high Na content is predicted for $[I]/[III] \leq 0.88$. Close to the back contact a high Na concentration is anticipated for $[I]/[III] \leq 0.83$, but no Na agglomeration should be detected for $[I]/[III] \geq 0.88$ (compare Figure S5, Supporting Information). To reveal the Na depth profiles, glow discharge optical emission spectroscopy (GDOES) was measured on all samples with constant $[Ag]/[I] = 0.8$ and $[Ga]/[III] = 0.85$. The depth distributions of Na and Ag, adjusted to the onset of the Ag signal, are shown in Figure 9a. The onset of the Mo signal from the back contact, which can be determined very precisely, is marked for each sample.

Obviously, the Na profiles correlate very well with the expected occurrence of OVC patches. Accordingly, the Ag signals for samples with $[I]/[III] \leq 0.88$ are reduced in the regions where the OVCs (i.e., lower Ag content) are observed. In the middle of the absorber the Na level is relatively comparable for all samples. Close to the back contact the Na signal increases already in the absorber (i.e., in the OVCs) for $[I]/[III] \leq 0.83$, while for higher $[I]/[III]$ ratios it does not increase until the Mo back contact (Na reservoir) is reached. This agrees with the STEM-EDS and Raman results, confirming OVCs at the back contact for all samples with $[I]/[III] \leq 0.83$. The by far highest Na concentration at the back contact for $[I]/[III] = 0.81$ is further in line with the largest OVC signal measured at the back of this absorber (Figure S5, Supporting Information). Why this particular sample actually showed this feature is not understood at this stage. It may indicate a strong sensitivity of the OVC formation to small (run-to-run) deviations in absorber processing (e.g., small lateral deviations in NaF thickness). The [I]-rich sample shows a narrow Na peak at the CdS/ACIGS interface. For $[I]/[III] = 0.96$, the same peak but with a shoulder toward the absorber is visible, which is in line with the (weak) OVC signal in Raman. For $[I]/[III] \leq 0.88$, this peak at the buffer interface disappears, but the Na signal expands deeper into the upper part of the absorber, which is

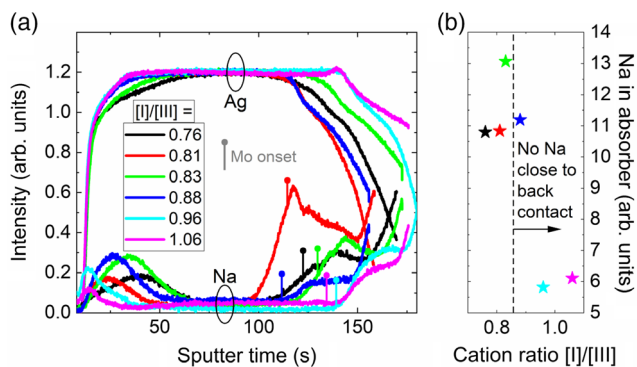


Figure 9. a) Ag and Na depth profiles as measured by GDOES for samples with different $[I]/[III]$ ratios and constant $[Ag]/[I] = 0.8$ and $[Ga]/[III] = 0.85$. The onset of the Mo signal is marked for each sample. b) Corresponding total Na intensity, integrated from the onset of the Ag to the onset of the Mo signal.

again justified by the existence of OVCs. It is proposed that the Na agglomeration at the buffer/absorber interface is considerably reduced for [I]-poor samples because the OVCs act as a “sponge” for Na. This would need to be taken into account when optimizing the Na supply during absorber processing. Figure 9b shows the integrated Na signal (from Ag to Mo onset) as a function of $[I]/[III]$. The increased Na incorporation for absorbers with a distinct OVC formation is obvious. However, it is not understood at this stage why the Na level in the absorber seems to saturate for $[I]/[III] \leq 0.88$, although microstructural and chemical analysis (see Figure 6 and 7) indicate a significantly lower OVC fraction for $[I]/[III] = 0.88$ as compared with $[I]/[III] = 0.76$. A possible explanation may be that the OVCs are not saturated in Na and/or that the Na transport to the OVC patches plays a role as well. For the future, atom probe tomography investigations are planned to directly visualize and quantify the Na segregation in OVCs, as it was done for K in CIGS before.^[53]

In summary, the observed Na accumulation in OVCs is in line with the proposed mechanisms, explaining the evolution of a transport barrier and the hysteresis effect for samples with $[Ag]/[I] = 0.8$. However, a result that strongly contradicts the latter rationale is that even the sample with no or only very minor OVC fraction ($[I]/[III] = 0.96$) showed a clear hysteresis effect (see Figure 4). If there would be a direct correlation, a significantly lower impact on sweep direction would have been expected for the near-stoichiometric sample. Thus, other origins, like, e.g., changing charge states of electronic defects upon voltage bias or a generally faster diffusion and drift of Na ions in the Ag-rich chalcopyrite lattice, are deemed more likely. Unpublished results (manuscript under preparation) show that the alkali solubility in ACIGS is increasing with increasing Ag content, which is in line with observations from earlier studies.^[32,54] Thus, a higher Na concentration and mobility are expected for higher levels of Ag alloying (unit cell size increases^[55]), which points toward the latter explanation. However, it remains to be revealed how the drift or displacement of Na ions affects the charge transport in detail.

Another aspect that needs to be studied in the future is if near-stoichiometric ACIGS absorbers with very minor OVC formation (like for the sample with $[I]/[III] = 0.96$) also show long-term degradation or if this effect is indeed exclusively linked to the presence/amount of OVCs. Furthermore, it remains unclear why the sample with $[Ag]/[I] = 0.8$ and $[Ga]/[III] = 0.72$ showed no blocking initially and a transport barrier only evolved over time, although the formation of OVCs at room temperature is deemed very unlikely.

2.4. Wider Perspective on OVC Formation in ACIGS System

In the final section of this work, the general tendency to OVC formation in the ACIGS system is discussed to complement the experimental results. A high tolerance to off-stoichiometry (i.e., extended 1:1:2 single-phase region) is found for the entire CIGS system, presumably mediated by the formation of highly stable $(2V_{Cu} + III_{Cu})$ defect complexes.^[39,56] The distribution of complexes always adheres to the concepts of minimum deviation from the octet rule.^[57] When the composition is near 1:1:2

stoichiometry, the concentration of defect complexes is small, and therefore entropy spreads them out evenly through the absorber volume. Even if some degree of clustering occurs, the conformations would be separated and randomly orientated. However, when the stoichiometry during deposition/upon cooling falls below a critical $[I]/[III]$ value, more of these complexes must fit into the same volume, and therefore they begin to interact and aggregate in separated regions to form ordered vacancy compounds. For CIGS films, formation of OVCs with constant 1:3:5 and/or 1:5:8 stoichiometry is confirmed.^[38] However, phase diagrams of the $Ag_2Se-In_2Se_3$ and $Ag_2Se-Ga_2Se_3$ systems indicate a reduced 1:1:2 single-phase region, being particularly narrow for $AgGaSe_2$.^[28,47] In both systems, only OVCs with 1:5:8 stoichiometry are clearly detected,^[28,47] although formation of $AgIn_3Se_5$ is suggested in some studies.^[45,46] The results from this work suggest that already a small Cu addition allows the formation of 1:3:5 OVCs in ACIGS films with high Ag and Ga concentrations. The effect might be promoted by the observed preference of Cu to fill OVCs, resulting in lower $[Ag]/[I]$ in 1:3:5 than in the surrounding 1:1:2 phase. The absence of the 1:3:5 OVC in the Ag–Ga–Se system may be connected to its negligible tolerance to off-stoichiometry. Similarly, a very narrow 1:1:2 region was observed for the Cu–In–S system, in which no 1:3:5 OVCs exist either.^[37,56]

Simchi et al.^[58] and Boyle et al.^[59] measured X-ray diffraction (XRD) (in the first case at grazing incidence [GI-XRD]) on sets of samples with varying $[Ag]/[I]$ and $[Ga]/[III]$. They found a secondary peak for 2θ angles roughly 0.8° higher than the (112) reflection for almost all samples lying in the compositional range of $[Ag]/[I] \geq 0.74$ and $[Ga]/[III] \geq 0.5$. The authors ascribed this signature to a 1:5:8 OVC at the absorber surface. For lower Ag and Ga contents, the OVC signal was not measured. The investigated compositions are shown in **Figure 10a** together with the compositions of absorbers evaluated by Raman in this study (see Figure 2 and Figure 5). Compositional regions for which either a clear or a negligible OVC formation is detected are enclosed by gray broken lines (assuming low OVC formation

for pure $CuInSe_2$ and $CuGaSe_2$). Outside these regions the situation is unknown. The appearance of OVCs obviously depends on the $[I]/[III]$ ratio of the respective samples. However, all samples shown in Figure 10a lie in a range of $0.8 \leq [I]/[III] \leq 0.95$ (for $[Ag]/[I] = 0.8$ and $[Ga]/[III] = 0.85$, one of the samples with $0.81 \leq [I]/[III] \leq 0.88$ can be chosen from Figure 5 for a fair comparison). Analysis of the GI-XRD (literature) and Raman (this study) results indicates that both signatures originate from the same OVC compound. The elemental quantification of the OVCs in this study indicates that these rather show a 1:3:5 than a 1:5:8 stoichiometry. Interestingly, for $AgIn_{0.5}Ga_{0.5}Se_2$ and $Ag_{0.74}Cu_{0.26}GaSe_2$, no OVCs were measured in (GI-)XRD.^[58,59] This may be attributed either to a near-perfect stoichiometry ($[I]/[III] > 0.9$) for these samples and/or, in the latter case, to the nonexistence of a 1:3:5 phase. To clarify if a continuous trend in OVC fraction with increasing Ag content exists in the full $[Ag]/[I]$ range, two additional samples with $[Ag]/[I] = 0$ ($[I]/[III] = 0.84$) and 1 ($[I]/[III] = 0.83$), both with $[Ga]/[III] = 0.85$, were processed. This allows to compare five samples with very similar integral off-stoichiometry ($[I]/[III] = 0.80–0.84$). Subsequent Raman analysis of the top surface revealed an increasing OVC amount with increasing Ag content for $[Ag]/[I] \geq 0.5$ (see Figure S10, Supporting Information). The pure AIGS sample exhibits by far the largest OVC signal.

The gathered experimental evidence suggests an increasing tendency to OVC formation toward high Ga and Ag contents, ultimately inducing the very narrow single-phase region of $AgGaSe_2$. Figure 10b shows the c/a lattice constant ratio of the entire chalcopyrite ACIGS alloy system, as extracted from 2D linear interpolation from experimental values of the ternary compounds.^[60,61] The results fit well with measured values for ACIGS and CIGS with intermediate compositions.^[55,59,61] A perfectly tetragonal ratio of $c/a = 2$ only occurs for quite low Ga and Ag contents. With increasing Ga and Ag concentrations, the tetragonal lattice is gradually distorted by compression along the c -axis. In first approximation, the decrease in the c/a ratio

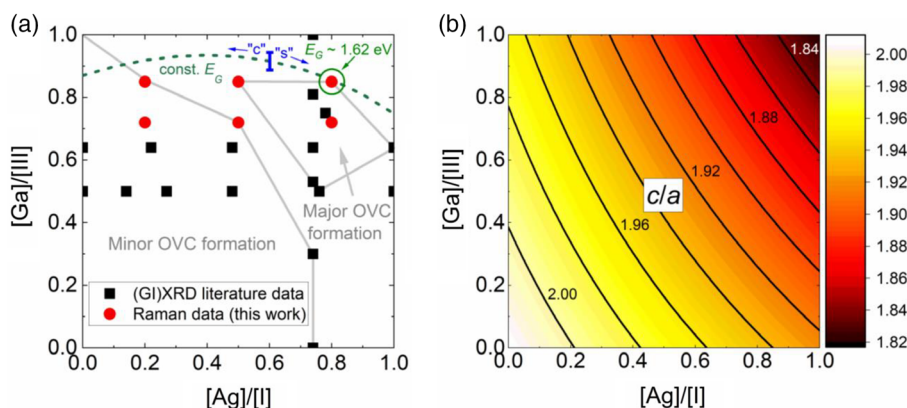


Figure 10. a) Integral ACIGS compositions of samples that were investigated by (GI)XRD in refs. [58,59] and by Raman spectroscopy in this study. All samples exhibit $[I]/[III]$ values in the range of $[I]/[III] = 0.8–0.95$. The samples for which either a clear or no/very minor OVC signature was observed are enclosed by gray broken lines. The dashed green line illustrates the compositions with constant $E_G \approx 1.62$ eV, which is reached for the sample marked by the green circle. The blue bar indicates the $[Ag]/[I]$ ratio for which a change from a cliff to a spike configuration at the CdS/ACIGS interface is predicted for this bandgap.^[2] b) Tetragonal distortion ($c/a \neq 2$) for the entire ACIGS system, as extracted from 2D linear interpolation between the reported experimental c/a values of the ternary compounds.^[60,61]

and the tendency to OVC formation follow the same compositional trend. Thus, the following simplified scenario is suggested: With increasing tetragonal distortion (i.e., decreasing c/a ratio), the interatomic distances and bond properties become increasingly dissimilar with respect to the bond orientation. As a result, a random distribution of $(2V_1 + III_1)$ defect complexes at near-stoichiometric compositions becomes energetically less favorable. The OVC is characterized by the preferential ordering of defects in planes perpendicular to c -axis.^[57] As such, stability of this phase is expected to be less impacted by the lattice distortion, simply because the bonds comprising it are less skewed. In practice, the relative stabilization of OVCs is manifested as the significantly increased tendency to form a mixture of OVC and 1:1:2 phases in place of off-stoichiometric chalcopyrite with random distribution/orientation of defect complexes, explaining the lower tolerance to off-stoichiometry. Comparing the experimental results with the extrapolated lattice distortions, a value of $c/a \leq 1.90$ may be a threshold for extensive OVC formation. It should be stressed though that the exact mechanism is more complex and its elucidation is not the aim of this work.

The green dashed line in Figure 10a shows the absorber compositions resulting in the same optimum top cell bandgap of ≈ 1.62 eV (formula from ref. [2]), as it is reached for the sample with $[Ag]/[I] = 0.8$ and $[Ga]/[III] = 0.85$ from this study (marked by green circle). However, the presented results clearly show that OVC formation is hard to avoid for this absorber composition. The presence of OVCs potentially deteriorates the initial performance and may apparently also cause long-term degradation (see Figure 1). Ultimately, the very narrow process window is a fundamental obstacle that may impede production on large areas. Thus, one may think of decreasing the tetragonal distortion by going to slightly Ag-poorer compositions and adjusting the Ga content accordingly to reach the optimum bandgap (e.g., $[Ag]/[I] \approx 0.2$ and $[Ga]/[III] \approx 0.9$). However, for $[Ag]/[I] < 0.6$, a change from a spike to a cliff configuration ("s" and "c" in Figure 10a) at the CdS/ACIGS interface is predicted for a constant $E_G = 1.62$ eV,^[2] which presumably increases interface recombination with decreasing Ag content. A possible way to circumvent this issue is to use alternative buffer materials with a lower electron affinity. For instance, by using an optimized ZTO buffer layer a positive CBO can be created with a significantly lower amount of Ag ($[Ag]/[I] \approx 0.4$),^[2] and thus lower tendency to OVC formation.

Further studies are recommended, focusing on *elimination of the OVCs* by hitting the perfect stoichiometry without forming other secondary phases or by widening the 1:1:2 single-phase region, as it was suggested with Na addition in CIGS.^[62] However, other works indicate a catalyzed OVC formation in CuInSe₂ by the presence of Na.^[63] In future experiments it is planned to systematically vary the NaF amount, which was previously optimized for pure CIGS and not for the ACIGS films in this study. First results (not shown here) indicate that using thinner NaF precursor layers may mitigate the OVC formation, at least at the back contact. An alternative would be to *suppress the detrimental character of the OVCs* by tailoring metal evaporation rates during deposition, thereby avoiding their appearance at the interfaces for absorbers with Ag- and Ga-rich compositions. In either

case, significant modification of the baseline absorber processing would be required.

3. Conclusion

This work highlights the paramount role of absorber stoichiometry in wide-gap ACIGS solar cells. To reach bandgap energies suitable for top cells in a tandem device, a $[Ga]/[III]$ ratio > 0.8 is necessary. At such high Ga concentrations, DFT calculations predict a beneficial, positive CBO at the CdS/ACIGS interface only for substantial Ag alloying of $[Ag]/[III] > 0.6$. However, the presented results illustrate that absorbers in this compositional range demonstrate a significantly increased tendency to OVC formation. This is exemplified for solar cell samples with a constant $[Ga]/[III] = 0.85$ and $[Ag]/[I] = 0.80$ but different off-stoichiometry ($0.76 \leq [I]/[III] \leq 1.06$). Absorbers with $[I]/[III] \leq 0.83$ contain large 1:3:5 OVC patches at the front and back contact, which show a significantly reduced $[Ag]/[I]$ ratio and are either Ga- or In-enriched. Corresponding solar cells exhibit a distinct barrier for current transport (related to OVCs at the back) and a wavelength-independent reduction in carrier collection (caused by OVCs at the front). For near-stoichiometric compositions, OVCs are only detected at the front surface, resulting in less distorted I - V characteristics. However, although solar cells with $[I]/[III] = 0.96$ show the highest J_{SC} , the FF starts to decline when approaching perfect stoichiometry, presumably due to the formation of Ag₃GaSe₆ precipitates. Consequently, the highest efficiency of 10.2% (without ARC) was measured for $[I]/[III] = 0.88$ and a bandgap of 1.63 eV. It is further revealed that solar cells with such high Ag and Ga contents display a strong hysteresis in I - V characteristics, with increased FF and V_{OC} values at reverse voltage sweep. This is not observed for $[Ga]/[III] \leq 0.85$ and $[Ag]/[I] \leq 0.5$. It is proposed that the hysteresis effect is attributed to the drift of mobile Na ions in the (1:1:2) absorber matrix upon voltage sweep, which is facilitated for ACIGS with high Ag content. Finally, the results indicate that the low tolerance to off-stoichiometry (i.e., massive formation of OVCs) deteriorates the long-term stability for absorbers with $[Ga]/[III] \geq 0.72$ and $[Ag]/[I] = 0.80$.

In summary, this study emphasizes the challenges of Ag alloying in chalcopyrite absorbers to increase the performance of wide-gap ACIGS solar cells with CdS buffer layers. If the detrimental character of the OVCs cannot be mitigated, they need to be avoided altogether. Possible strategies may be fast cool-down rates (wider single-phase region at high temperatures) or a broadening of the single-phase region at room temperature (e.g., by introducing extrinsic elements like heavy alkali metals).

4. Experimental Section

Solar Cell Processing: The solar cells in this study were produced in the following stack sequence: soda lime glass (SLG)/Mo/NaF/ACIGS/CdS/i-ZnO/ZnO:Al. First, the Mo back contact was sputtered (DC) on the SLG substrates, followed by evaporation of ≈ 10 nm of NaF (no alkali diffusion-barrier was used). Subsequently, ACIGS absorber films were grown by a three-stage ([I]-poor \rightarrow [I]-rich \rightarrow [I]-poor) coevaporation process, without changing the Ag/Cu evaporation rate ratio at any deposition time. During initial absorber growth, an increased Ga/In evaporation rate ratio was set to implement a back-surface field. The maximum substrate

temperature was set to 550 °C. No alkali postdeposition treatment (PDT) was applied. The estimated absorber compositions for the samples in the first part of this study, i.e., with varying Ag and Ga contents, are shown in Figure 1. For further details, we refer to ref. [2]. For the second part of this work, the [I]/[III] ratio was varied in the range of $0.76 \leq [I]/[III] \leq 1.06$, with a constant composition of $[Ga]/[III] = 0.85 \pm 0.01$ and $[Ag]/[I] = 0.80 \pm 0.02$. The integral compositions were extracted from cross-calibrated X-ray fluorescence measurements on the bare absorbers. All ACIGS films exhibit very similar elemental depth profiles, akin to the ones in ref. [2], and the thickness is $2.1 \pm 0.2 \mu\text{m}$. After absorber deposition, a 50 nm-thick CdS buffer layer was grown by chemical bath deposition. The solar cell stacks were finalized by sputtering i-ZnO (70 nm) and ZnO:Al (150 nm; sheet resistance $\approx 50 \Omega \text{sq}^{-1}$) on top. Finally, all samples were sectioned by mechanical scribing into 25 solar cells with an area of 0.05 cm^2 each.

Microstructural and Chemical Absorber Characterization: STEM on a FEI Titan Themis XFEI instrument assisted by EDS allowed for identification of OVC patches and quantification of absorber compositions. The TEM lamellae were prepared via focused ion beam and subsequent liftoff. Phase identification of the absorber surface region was facilitated by Raman spectroscopy (Renishaw inVia) using a laser with 532 nm excitation wavelength ($\approx 200 \text{ nm}$ probing depth) at $20\times$ magnification. Elemental depth profiling, integrated over a large area ($\approx 6 \text{ mm}^2$), was conducted by GDOES, using a Spectrums Analytik GDA 750HR system. SEM analysis, utilizing a Zeiss Merlin instrument ($V_{\text{acc}} = 5 \text{ kV}$), was used to investigate the solar cell cross sections and identify differences in microstructure.

Characterization of Solar Cells: Completed solar cells were characterized by EQE and I - V measurements at $T = 25^\circ\text{C}$ and under illumination by an ELH lamp in home-built setups. The light intensity during I - V analysis was calibrated for each sample to the $J_{\text{SC,EQE}}$ value, deduced from EQE by calculating the simulated short circuit current density under illumination with the AM1.5G spectrum.

Supporting Information

Supporting Information is available from the Wiley Online Library or from the author.

Acknowledgements

This work was supported by the Swedish Foundation for Strategic Research (SSF) under the project number RMA15-0030 and by the Swedish Energy Agency under the project number P43238-1, Dnr 2016-008376.

Conflict of Interest

The authors declare no conflict of interest.

Keywords

(Ag,Cu)(In,Ga)Se₂, Cu(In,Ga)Se₂, ordered vacancy compounds, stoichiometry, wide-gap chalcopyrite

Received: August 21, 2020

Revised: September 12, 2020

Published online: September 29, 2020

- [1] A. S. Brown, M. A. Green, *Physica E* **2002**, 14, 96.
- [2] J. Keller, K. V. Sopiha, O. Stolt, L. Stolt, C. Persson, J. J. S. Scragg, T. Törndahl, M. Edoff, *Prog. Photovoltaics Res. Appl.* **2020**, 28, 237.

- [3] A. Yamada, K. Matsubara, S. Nakamura, S. Ishizuka, K. Sakurai, H. Tampo, H. Shibata, H. Nakanishi, S. Niki, *Phys. Status Solidi A* **2006**, 203, 2639.
- [4] S.-H. Wei, A. Zunger, *J. Appl. Phys.* **1995**, 78, 3846.
- [5] J. Keller, O. V. Bilousov, J. Neerken, E. Wallin, N. M. Martin, L. Riekehr, M. Edoff, C. Platzer-Björkman, *Sol. RRL* **2020**, 4, 2000248.
- [6] T. Feurer, F. Fu, T. P. Weiss, E. Avancini, J. Löckinger, S. Buecheler, A. N. Tiwari, *Thin Solid Films* **2019**, 670, 34.
- [7] F. Larsson, N. S. Nilsson, J. Keller, C. Frisk, V. Kosyak, M. Edoff, T. Törndahl, *Prog. Photovolt. Res. Appl.* **2017**, 25, 755.
- [8] M. A. Contreras, L. M. Mansfield, B. Egaas, J. Li, M. Romero, R. Noufi, E. Rudiger-Voigt, W. Mannstadt, *Prog. Photovolt. Res. Appl.* **2012**, 20, 843.
- [9] A. Jasenek, U. Rau, V. Nadenau, H. W. Schock, *J. Appl. Phys.* **2000**, 87, 594.
- [10] V. Nadenau, U. Rau, A. Jasenek, H. W. Schock, *J. Appl. Phys.* **2000**, 87, 584.
- [11] M. Gloeckler, J. R. Sites, *Thin Solid Films* **2005**, 480–481, 241.
- [12] B. Huang, S. Chen, H. Deng, L. Wang, M. A. Contreras, R. Noufi, S.-H. Wei, *IEEE J. Photovoltaics* **2014**, 4, 477.
- [13] J. Pohl, K. Albe, *Phys. Rev. B* **2013**, 87, 245203.
- [14] C. Spindler, F. Babbe, M. H. Wolter, F. Ehre, K. Santosh, P. Hilgert, F. Werner, S. Siebentritt, *Phys. Rev. Mater.* **2019**, 3, 090302.
- [15] C. Spindler, D. Regesch, S. Siebentritt, *Appl. Phys. Lett.* **2016**, 109, 032105.
- [16] G. Hanna, A. Jasenek, U. Rau, H. W. Schock, *Thin Solid Films* **2001**, 387, 71.
- [17] G. Hanna, A. Jasenek, U. Rau, H. W. Schock, *Phys. Status Solidi A* **2000**, 179, 73.
- [18] M. Raghuwanshi, E. Cadel, P. Pareige, S. Duguay, F. Couzinie-Devy, L. Arzel, N. Barreau, *Appl. Phys. Lett.* **2014**, 105, 013902.
- [19] J. Lindahl, J. Keller, O. Donzel-Gargand, P. Szaniawski, M. Edoff, T. Törndahl, *Sol. Energy Mater. Sol. Cells* **2016**, 144, 684.
- [20] G. M. Hanket, J. H. Boyle, W. N. Shafarman, in *34th IEEE Photovoltaic Specialists Conf.*, IEEE, Philadelphia, PA **2009**, pp. 001240–001245.
- [21] T. Nakada, K. Yamada, R. Arai, H. Ishizaki, N. Yamada, *MRS Proc.* **2005**, 865, F11.1.
- [22] T. Umehara, F. Zulkifly, K. Nakada, A. Yamada, *Jpn. J. Appl. Phys.* **2017**, 56, 08MC09.
- [23] K. V. Sopiha, J. K. Larsen, O. Donzel-Gargand, F. Khavari, J. Keller, M. Edoff, C. Platzer-Björkman, C. Persson, J. J. S. Scragg, *J. Mater. Chem. A* **2020**, 8, 8740.
- [24] T. Wada, N. Kohara, S. Nishiwaki, T. Negami, *Thin Solid Films* **2001**, 387, 118.
- [25] Y. Ema, H. Kato, T. Takahashi, *Jpn. J. Appl. Phys.* **2002**, 41, 1527.
- [26] S. Soltanmohammad, W. N. Shafarman, *Sol. Energy Mater. Sol. Cells* **2018**, 182, 142.
- [27] A. Virtuani, E. Lotter, M. Powalla, U. Rau, J. H. Werner, M. Acciarri, *J. Appl. Phys.* **2006**, 99, 014906.
- [28] J. C. Mikkelsen, *Mater. Res. Bull.* **1977**, 12, 497.
- [29] S. Lin, W. Li, S. Li, X. Zhang, Z. Chen, Y. Xu, Y. Chen, Y. Pei, *Joule* **2017**, 1, 816.
- [30] G. M. Hanket, J. H. Boyle, W. N. Shafarman, G. Teeter, in *35th IEEE Photovoltaic Specialists Conf.*, IEEE, Honolulu, HI **2010**, pp. 003425–003429.
- [31] W. Shafarman, C. Thompson, J. Boyle, G. Hanket, P. Erslev, J. D. Cohen, in *IEEE Photovoltaic Specialists Conf.*, IEEE, Honolulu, HI **2010**, pp. 325–329.
- [32] K. Kim, S. K. Ahn, J. H. Choi, J. Yoo, Y. J. Eo, J. S. Cho, A. Cho, J. Gwak, S. Song, D. H. Cho, Y. D. Chung, J. H. Yun, *Nano Energy* **2018**, 48, 345.
- [33] T. Kato, J. Wu, Y. Hirai, H. Sugimoto, V. Bermudez, *IEEE J. Photovoltaics* **2019**, 9, 325.

- [34] S. Meloni, T. Moehl, W. Tress, M. Franckeviius, M. Saliba, Y. H. Lee, P. Gao, M. K. Nazeeruddin, S. M. Zakeeruddin, U. Rothlisberger, M. Graetzel, *Nat. Commun.* **2016**, 7, 10334.
- [35] R. Wuerz, W. Hempel, P. Jackson, *J. Appl. Phys.* **2018**, 124, 165305.
- [36] M. Malitckaya, H.-P. Komsa, V. Havu, M. J. Puska, *J. Phys. Chem. C* **2017**, 121, 15516.
- [37] J. Keller, O. V. Bilousov, E. Wallin, O. Lundberg, J. Neerken, S. Heise, L. Riekehr, M. Edoff, C. Platzer-Björkman, *Phys. Status Solidi A* **2019**, 216, 1900472.
- [38] M. Grossberg, J. Krustok, S. Siebentritt, J. Albert, *Phys. B Condens. Matter* **2009**, 404, 1984.
- [39] S. B. Zhang, S.-H. Wei, A. Zunger, H. Katayama-Yoshida, *Phys. Rev. Appl.* **1999**, 60, 1865.
- [40] K. Ueda, T. Maeda, T. Wada, *Thin Solid Films* **2017**, 633, 23.
- [41] T. Maeda, W. Gong, T. Wada, *Curr. Opin. Green Sustain. Chem.* **2017**, 4, 77.
- [42] A. Sharan, F. P. Sabino, A. Janotti, N. Gaillard, T. Ogitsu, J. B. Varley, *J. Appl. Phys.* **2020**, 127, 065303.
- [43] T. Negami, N. Kohara, M. Nishitani, T. Wada, T. Hirao, *J. Appl. Phys.* **1995**, 825, 6.
- [44] S. Levchenko, N. N. Syrbu, A. Nateprov, E. Arushanov, J. M. Merino, M. León, *J. Phys. D. Appl. Phys.* **2006**, 39, 1515.
- [45] O. Yarema, M. Yarema, V. Wood, *Chem. Mater.* **2018**, 30, 1446.
- [46] O. Yarema, M. Yarema, D. Bozyigit, W. M. M. Lin, V. Wood, *ACS Nano* **2015**, 9, 11134.
- [47] I. A. Ivashchenko, I. V. Danyliuk, I. D. Olekseyuk, V. V. Halyan, *J. Solid State Chem.* **2014**, 210, 102.
- [48] H. Ishizaki, K. Yamada, R. Arai, Y. Kuromiya, Y. Masatsugu, N. Yamada, T. Nakada, *Mater. Res. Soc. Symp. Proc.* **2005**, 865, 143.
- [49] F. Pianezzi, P. Reinhard, A. Chirilă, B. Bissig, S. Nishiwaki, S. Buecheler, A. N. Tiwari, *Phys. Chem. Chem. Phys.* **2014**, 16, 8843.
- [50] J.-H. Yoon, J.-H. Kim, W. M. Kim, J.-K. Park, Y.-J. Baik, T.-Y. Seong, J. Jeong, *Prog. Photovolt. Res. Appl.* **2014**, 22, 90.
- [51] H. Simchi, B. McCandless, W. Shafarman, K. Kim, J. Boyle, R. Birkmire, in *37th IEEE Photovoltaics Specialist Conf.*, IEEE, Seattle, WA **2011**, pp. 000041–000045.
- [52] H. Simchi, B. E. McCandless, K. Kim, J. H. Boyle, R. W. Birkmire, W. N. Shafarman, *IEEE J. Photovoltaics* **2012**, 2, 519.
- [53] A. Stokes, M. Al-Jassim, A. Norman, D. Diercks, B. Gorman, *Prog. Photovoltaics Res. Appl.* **2017**, 25, 764.
- [54] K. Kim, J. W. Park, J. S. Yoo, J. S. Cho, H. D. Lee, J. H. Yun, *Sol. Energy Mater. Sol. Cells.* **2016**, 146, 114.
- [55] J. H. Boyle, B. E. McCandless, W. N. Shafarman, R. W. Birkmire, *J. Appl. Phys.* **2014**, 115, 223504.
- [56] C. Stephan, Ph.D. Thesis, Freie University, Berlin, Germany **2011**.
- [57] S. B. Zhang, S. Wei, A. Zunger, H. Katayama-Yoshida, *Phys. Rev. B* **1998**, 57, 9642.
- [58] H. Simchi, B. McCandless, W. Shafarman, K. Kim, J. Boyle, R. Birkmire, in *37th IEEE Photovoltaics Specialist Conf.*, IEEE, Seattle, WA **2011**, pp. 000041–000041.
- [59] J. H. Boyle, B. E. McCandless, G. M. Hanket, W. N. Shafarman, *Thin Solid Films* **2011**, 519, 7292.
- [60] J. J. M. Binsma, L. J. Giling, J. Bloem, *Phys. Status Solidi A* **1981**, 63, 595.
- [61] M. R. Balboul, H. W. Schock, S. A. Fayak, A. A. El-Aal, J. H. Werner, A. A. Ramadan, *Appl. Phys. A* **2008**, 92, 557.
- [62] R. Herberholz, U. Rau, H. W. Schock, T. Haalboom, T. Gödecke, F. Ernst, C. Beilharz, K. W. Benz, D. Cahen, *EPJ Appl. Phys.* **1999**, 6, 131.
- [63] T. Tanaka, Y. Demizu, A. Yoshida, T. Yamaguchi, *J. Appl. Phys.* **1997**, 81, 7619.